Segmentation of the mouse fourth deep lumbrical muscle connectome reveals concentric organization of motor units

Please cite this article as: Hirst, T. C., & Ribchester, R. R. (2013). Segmentation of the mouse fourth deep lumbrical muscle connectome reveals concentric organization of motor units. Journal of Physiology, doi: 10.1113/jphysiol.2013.258087
This is a PDF file of an unedited manuscript that has been accepted for publication.

Segmentation of the mouse fourth deep lumbrical muscle connectome reveals concentric organisation of motor units

Theodore C. Hirst and Richard R. Ribchester*

Euan MacDonald Centre for Motor Neurone Disease Research, Centre for Integrative Physiology, Hugh Robson Building, University of Edinburgh, Edinburgh, EH8 9XD, UK

Running title: The mouse 4DL connectome

Keywords: Motor unit, neuromuscular junction, confocal microscopy

Word count: 7122

* *to whom correspondence should be addressed:*
Professor Richard R Ribchester
Euan Macdonald Centre for Motor Neurone Disease Research
Centre for Integrative Physiology
The University of Edinburgh
Edinburgh
EH8 9XD
UK
Email: rrr@ed.ac.uk
Tel: 01316503256

KEY POINTS SUMMARY

-An accelerated image segmentation algorithm was developed and applied to analysis of motor unit arborisation and connectivity (the “connectome”) in fourth deep lumbrical muscles (4DL) of mice expressing Fluorescent Proteins as morphological reporters

-Mouse 4DL muscles contain between 4 and 9 motor units and motor unit size in these muscles ranged from 3-111 muscle fibres

-Small motor units were restricted in their arbors to the vicinity of the nerve entry point. Larger motor units concentrically occupied muscle fibres located progressively further from the nerve entry point

-Motor unit size was weakly correlated with motor endplate size, suggesting a hierarchy of motor unit sizes based on synaptic strength

-The data suggest a segregated organization of motor units in cylindrical muscles that has not previously been appreciated and indicate the direction of future studies required to establish possible relationships between the strengths of synaptic connections and motor unit size

ABSTRACT

Connectomic analysis of the nervous system aims to discover and establish principles that underpin normal and abnormal neural connectivity and function. Here we performed image analysis of motor unit connectivity in the fourth deep lumbrical muscle (4DL) of mice, using transgenic expression of fluorescent protein in motor neurones as a morphological reporter. We developed a method that accelerated segmentation of confocal image projections of 4DL motor units, by applying high resolution (63x 1.4NA objective) imaging or deconvolution only where either proved necessary, in order to resolve axon crossings that produced ambiguities in the correct assignment of axon terminals to identified motor units imaged at lower optical resolution (40x, 1.3NA). The 4DL muscles contained between 4 and 9 motor units and motor unit sizes ranged in distribution from 3 to 111 motor nerve terminals per unit. Several structural properties of the motor units were consistent with those reported in other muscles, including suboptimal wiring length and distribution of motor unit size. Surprisingly, however, small motor units were confined to a region of the muscle near the nerve entry point, whereas their larger counterparts were progressively more widely dispersed, suggesting a previously unrecognised form of segregated motor innervation in this muscle. We also found small but significant differences in variance of motor endplate length in motor units, which correlated weakly with their motor unit size. Thus, our connectomic analysis has revealed a pattern of concentric innervation that may perhaps also exist in other, cylindrical muscles that have not previously thought to show segregated motor unit organisation. This organisation may be the outcome of competition during postnatal development based on intrinsic neuronal differences in synaptic size or synaptic strength that generates a territorial hierarchy in motor unit size and disposition.

ABBREVIATIONS:

4DL, 4^{th} deep lumbrical muscle; CFP, cyan fluorescent protein; FP, fluorescent protein; MIP, maximum intensity projection; NMJ, neuromuscular junction; TAL, total arbor length; TRITC-α-BTX, tetramethyl rhodamine isothiocyanate α-bungarotoxin; YFP, yellow fluorescent protein; YFP16, transgenic YFP mouse line 16; YFP-H, transgenic YFP mouse line H

INTRODUCTION

Higher functions of the nervous system are thought to emerge from the properties of its component neural systems and circuits, and to the disposition and strengths of the synaptic connections that these comprise (Churchland & Sejnowski, 1988; Lichtman & Denk, 2011). Thus, a goal of "connectomic" analysis of neural connectivity is to abstract accurate wiring diagrams of the nervous system and thereby to establish principles that both explain and predict the normal functions of neural circuits and systems. Deviation from presumptive canonical principles of neural circuit organisation or function might then help to explain a wide range of abnormalities or diseases, including disorders of cognition, emotion, motivation and behaviour.

Connectomic analysis of brain circuits presents daunting technical challenges of acquisition, analysis and archiving of the raw data. To date, a complete wiring diagram of a nervous system has only been obtained by serial sectioning and reconstruction in only one species: the nematode worm, *Caenorhabditis elegans* (White *et al.*, 1986). Additional progress has been made towards establishing principles of neuronal wiring in *Drosophila* (Meinertzhagen & Lee, 2012) and of mammalian nervous systems through studies of retinal organisation (Helmstaedter *et al.*, 2011; Kleinfeld *et al.*, 2011) and the peripheral connectivity of motor neurones with their skeletal muscle targets (Lu *et al.*, 2009). Thus far, the only mammalian muscle for which a complete connectomic analysis has been performed is the mouse interscutularis muscle (Lu *et al.*, 2009). It is important that such analysis is extended to other muscles because different kinds of skeletal muscles may differ in the principles that govern their motor unit organisation. For instance, physiological measurements of isometric twitch tension, or characterisation of motor unit size from the glycogen depletion in stimulated motor units suggest that motor unit size is more uniformly distributed in muscles containing predominantly 'slow-twitch' (Type I) muscle fibres than those containing 'fast-twitch' (Type II) fibres (Hennig & Lomo, 1985, 1987). Other forms of classification of muscle types based on their development or properties of their motor nerve supply also raise the possibility that different organising principles may be involved (Pun *et al.*, 2002; Murray *et al.*, 2008). Finally, some muscles have a clearly segregated innervation pattern, particularly those that are topographically arranged with respect to their nerve supply, such as the intercostals and other muscles supplied by sequential thoracic spinal segments and ventral roots; whereas muscles which are relatively cylindrical in form are not thought

to show any significant degree of segregated innervation, even where their motor nerve supply arises from separate spinal segments (Peyronnard & Charron, 1982). The motor units derived from contiguous spinal segments have been thought to intermingle their connections homogeneously in target muscles of this type.

The approach used previously, to establish the connectome of the interscutularis muscle (Lu *et al*., 2009), was evidently a painstaking one of serial optical sectioning using confocal laser scanning microscopy at maximum resolution of whole mounts of this muscle. This approach reportedly required weeks or months to procure and process sufficient data to enable comparison and testing of various hypotheses (Srinivasan *et al.*, 2010), including correspondence of motor unit branching between animals, bilateral symmetry; and whether branching patterns conform to principles of minimising branch lengths in complex circuits.

In the present study, we utilised a 'progressive resolution' method, which accelerated connectomic analysis, and we applied this to the fourth deep lumbrical (4DL) in mice. This muscle is also of proven neurophysiological interest because, in rodents such as rats and mice, its motor nerve supply arises from branches of the tibial and sural nerves, which anastomose near the ankle before providing a common motor nerve supply derived from a branch of the lateral plantar nerve (Nakanishi & Norris, 1970; Betz *et al.*, 1979; Taxt, 1983; Ribchester *et al.*, 2004; Teriakidis *et al.*, 2012). This anatomy has facilitated experiments that probe mechanisms of neuromuscular synaptic plasticity and competition (Ribchester & Taxt, 1983; Barry & Ribchester, 1995; Costanzo *et al.*, 2000). Superficially, motor units arising from contiguous ventral roots seem to be intermingled randomly, both within the two anatomically distinct nerve supplies and within the muscle itself (Betz *et al.*, 1979; Jones *et al.*, 1987; Ribchester, 1988; Betz *et al.*, 1990; Gates *et al.*, 1991; Gates & Ridge, 1992; Gates & Betz, 1993; Costanzo *et al.*, 2000; Gillingwater *et al.*, 2002). Insights into principles of motor unit organisation and its link to function in this muscle could therefore provide a foundation for exploring and understanding general principles and mechanisms of neuromuscular development, synaptic degeneration after nerve injury, or axon degeneration in models of motor neurone disease such as amyotrophic lateral sclerosis or spinal muscular atrophy (Gillingwater *et al.*, 2003; Gillingwater & Ribchester, 2003).

The connectomic analysis of 4DL we utilised in the present study confirmed several of the findings made by analysis of the interscutularis connectome reported previously

by Lu *et al.* but also highlighted a surprising and important difference from this thin, sheetlike muscle: non-random motor unit innervation. Specifically, we observed that the axon collaterals of small motor units in 4DL were concentrated in the vicinity of the intramuscular nerve entry point and larger motor units overlapped and extended concentrically beyond those. The concentric organisation of motor units in 4DL that we report here thus revealed a type of segregated innervation in a cylindrical muscle that has not been fully appreciated previously. Finally, we also found a weak association between motor nerve terminal size and motor unit size, which is consistent with one possible mechanism of motor unit segregation during competitive synapse elimination postnatally, namely on the basis of difference in synaptic strength (Buffelli *et al.*, 2003; Kasthuri & Lichtman, 2003), which is known to correlate with motor nerve terminal size in rodents (Harris & Ribchester, 1979; Costanzo *et al.*, 1999).

MATERIALS AND METHODS

Ethical approval

Experiments in this publication were carried out on transgenic mice in accordance with UK Home Office regulations under project license PPL60/3917.

Animals

Male and female mice (C57Bl/6 and C57Bl/6J) were drawn from breeding colonies in Edinburgh established respectively from stock obtained originally from Harlan-Olac (Oxford, UK) and The Jackson Laboratory (Bar Harbor, Maine, USA). Three transgenic mouse lines were used: two expressing YFP and one expressing CFP, all under the control of the *thy1.2* promoter (Feng *et al.*, 2000). The YFP lines were YFP16 (Jackson strain name: B6.Cg-Tg(Thy1-YFP)16Jrs/J), expressing YFP in 100% of motor neurons and YFP-H (B6.Cg-Tg(Thy1-YFP)HJrs/J), in which expression is limited to approximately 5%. CFP (B6.Cg-Tg(Thy1-CFP)23Jrs/J) is expressed in the majority of motor neurons. All the connectomic analysis was performed on the fourth deep lumbrical muscle (4DL) in the hind limb.

We dissected 76 muscles from 38 mice: 54 YFP-H, 10 YFP16 and 12 CFP. Of these, we discarded 43 YFP-H muscles because they contained no fluorescent motor neurons, due to the low penetrance of YFP expression in 4DL motor units of these transgenic mice, and could therefore not be used. We also discarded 16 other muscles (two YFP-H, five YFP16, nine CFP) because of damage to nerve fascicles or

poor FP expression, including the presence of non-fluorescent motor units in CFP muscles, which also show a lower penetrance of FP expression compared with the YFP16 transgenic line. During segmentation, a further five muscles (two YFP-H, two YFP16, one CFP) were excluded after discovery of small-scale damage or faint FP fluorescence, that was not evident on initial inspection. Thus, we successfully analysed seven YFP-H muscles and five full connectomes (three YFP16 and two CFP muscles), comprising a total of 41 motor units. YFP16/CFP muscles were innervated by a median of six motor units (range 4-9), and YFP-H muscles contained either one or two fluorescent motor units (three and four muscles respectively).

Tissue Dissection and labelling

Mice were sacrificed by cervical dislocation. The 4DL muscles were dissected and placed in buffered 0.1M phosphate buffer saline (PBS). Acetylcholine receptors were stained with tetramethyl rhodamine isothiocyanate α-bungarotoxin (TRITC-α-BTX, 5µg/ml; Invitrogen or Biotium, Inc.) in PBS for 20 minutes, fixed in 4% paraformaldehyde solution for 30 minutes, then mounted on slides in Vectashield mounting medium (Vector Laboratories). The preparations were gently squashed to reduce the mean distance between tissue and coverslip.

Confocal microscopy and image acquisition

Each muscle was first assessed using epifluorescence microscopy for fluorescent protein (FP) expression and structural integrity of motor unit arbors. Fifty-nine muscles were discarded because they either showed poor or absent FP expression, or contained broken intramuscular nerve fascicles.

The remaining 17 muscles, with fluorescent, intact innervation were imaged using a Zeiss LSM710 laser scanning confocal microscope. Objective lenses used for images acquired for analysis were 40x (Apochromat oil immersion: 1.3 NA) and 63x (Apochromat oil immersion; 1.4 NA). Images were acquired sequentially, with 2-line averaging. Where the thickness (z-axis) of the muscle was problematic, yielding weak fluorescence in deeper image slices, the microscope was set to increase gain with z-depth. This improved image contrast in the deeper layers of the muscle while preventing saturation superficially. Excitation of YFP, CFP and TRITC-α-BTX was obtained using 488, 440 and 548nm lines of the Argon and HeNe lasers. All images were acquired as 3D image stacks, at user-defined increments and with visually

defined upper and lower limits. Other image parameters (pixel and step size, pinhole size, dynamic range) for specific confocal setups are highlighted in sections below.

Image analysis and connectomic segmentation

For clarification, in this paper we use the term 'segmentation' in the conventional image-processing/analysis sense: that is, the digital isolation of one constituent structure from others comprising an image. By contrast, we use the term 'segmental innervation' to describe the biological organisation of nerve supply with respect to the spinal segments that originate the relevant peripheral nerve axons; and "segregated innervation" to indicate the separation of motor units within target muscles, irrespective of the spinal segmental origin of the axons.

We developed our motor unit segmentation protocol first using YFP-H muscles expressing either one or two fluorescent motor units (Fig. 1A). Once motor units could be successfully segmented and analysed with this method, we then applied it to YFP16 and CFP muscles (Fig. 1B), in which all or virtually all motor endplates were occupied by terminals belonging to fluorescent motor units. Rarely, we observed a few vacant endplates in YFP16 muscles but the incidence of these did not substantively impact on our analysis. Data obtained from YFP-H muscles were combined with YFP16 and CFP data for analysis, except where indicated.

YFP-H muscles

An initial image stack was acquired, aimed at containing the whole muscle within a single image at the highest resolution possible – this was done using the 40x objective lens. In order to capture the whole muscle, the microscope's 'tile scan' feature was utilised: a user-defined grid of adjacent stacks were acquired and automatically stitched together, within the Zeiss Zen user interface, to generate a single image. Images consisted of between 18 and 36 image stacks, depending on the size of the muscle. Image stacks for YFP or CFP and TRITC-α-BTX were acquired separately and combined later where required. For YFP and CFP, each image was acquired with pixel size of 210x210nm and a step size of 850nm, with 8-bit dynamic range. The pinhole was set between 1 and 1.5 Airy units, depending on the quality of FP fluorescence; where intensity was poor in the deeper layers of the muscle, the pinhole was opened slightly and these deeper layers were reimaged. For TRITC-α-BTX images, pixel size was doubled to 420x420nm, as optimal resolution

was not a key concern. Pinhole was kept at 1 Airy unit for all samples; all other parameters were as above.

The user (TH) then manually inspected the whole muscle and its axon branches for regions where 2 or more axons converged below the resolving power of the image – i.e. where the paths of axons could not be followed by eye reliably. These were termed 'areas of ambiguity'.

Each area of ambiguity was then cropped out of the image stack and deconvolved using the public license 'Parallel Iterative Deconvolution 3D' plugin (available at http://fiji.sc/wiki/index.php/Parallel_Iterative_Deconvolution) for Fiji ('Fiji Is Just ImageJ' pre-packaged with image processing software, http://pacific.mpi-cbg.de). We used a point-spread function (PSF) measured from the microscope using panfluorescent beads of diameter 100nm. A PSF was acquired for each set of confocal parameters (pixel size, step size, objective lens, pinhole size, laser) so that a suitable PSF was available for every image. The area was deemed resolved if the user could manually follow each axon branch through the area of ambiguity. Where deconvolution failed, areas of ambiguity were reimaged at the resolution limit of the confocal microscope, using the 63x objective lens. Single image stacks of only the YFP or CFP channel were acquired with pixel size of 130x130nm, step size of 380nm and 16-bit dynamic range. The pinhole was opened to 1 Airy unit. In both deconvolution and reacquisition, median filters (radius 2 pixels) and unsharp masks (radius 2 pixels, mask weight 0.3) were applied to reduce noise. If sufficient resolution was not acquired to resolve an area of ambiguity despite these steps, due to tissue damage, poor FP expression or otherwise, the sample was discarded (Fig. 1).

Once every area of ambiguity was resolved, the muscle was segmented by analysis of the original image stack. As a pre-processing step, for reasons related to the limited RAM in our image-analysing computer, each image was reduced such that its total size was between 300 and 500MB (typically, scaling by a factor of 0.5 in *xyz* dimensions). If a second image of the deeper layers of the muscle was acquired we replaced the relevant image slices. Axon branches were traced using the 'Simple Neurite Tracer' plugin for Fiji. At areas of ambiguity, the resolved secondary images (either deconvolved or 63x objective) were used to inform tracing in the original image. That is, in each secondary image, axons entering and leaving the area of ambiguity were identified in the original image and thus the area traced was that in the original image. Once segmentation was complete, a 3D skeleton of each motor

unit was generated using the ‘skeletonize’ tool in Fiji and these were assembled, as 2D maximum intensity projections (MIP), in Adobe Photoshop.

YFP-H muscles contained a median of 9 areas of ambiguity per muscle (IQR 6.5 - 11; range 2 - 15); 52.4% of these areas (32 out of 61) were deconvolved successfully. All remaining areas were resolved successfully with reimaging at high power.

YFP16 and CFP muscles

To produce full muscle connectomes from YFP16 or CFP muscles, the above protocol was modified to compensate for areas of ambiguity that were more difficult to resolve (Fig. 2A). If an area of ambiguity contained six or more incoming axons within the same fascicle, we described it as ‘complex’ (Fig. 2A, red box (online)); if there were fewer we described it as ‘simple’ (Fig. 2A, yellow box (online)). Despite such complexity, large areas of the muscle remained segmentable in the lower power image stack, even in the busier nerve fascicles (Fig. 2B,E). Simple areas of ambiguity were resolved in the same fashion as YFP-H areas – with a trial of deconvolution (compare Fig. 2C top left, before deconvolution; top right after deconvolution) and reimaging where necessary. For complex areas, deconvolution turned out to be less useful for resolving ambiguity. In these instances we reimaged using a 63x objective, with the same parameters described above (compare Fig. 2D top left, 40x objective; top right, 63x objective). Orthogonal projections (lower panels of Fig. 2C, D) further supported the resolution of ambiguity in axon identification by these methods. If axon convergence still remained ambiguous, we deconvolved the relevant area in this high power image. Finally if this failed to resolve the ambiguity, the sample was discarded (Fig. 1). Full connectomes were then segmented and rendered in the same way as YFP-H muscles.

In YFP16 and CFP muscles, there was a median of 37 (IQR 27 – 42; range 24 – 45) areas of ambiguity in each muscle, comprising medians of 12 (IQR 7 – 15; range 4 - 22) and 23 (IQR 20 – 30; range 12-30) simple and complex areas respectively. Deconvolution was successful in 82.2% of simple areas (Fig. 2B) and reimaging was 100% successful. Complex areas were successfully resolved with reimaging in 79.6% cases (Fig. 2C) and deconvolution of the high-resolution images was successful for the remainder. We found no instances of axon convergence that we were unable to resolve, requiring the sample to be discarded.

As expected, it took longer to segment full connectomes in YFP16/CFP muscles than segmentation of single or pairs of motor units in YFP-H muscles (YFP-16/CFP: 35.95 ± 5.90 hours (mean ± SD), range 28 – 44 vs. 5.28 ± 2.21 hours, range 2.5 – 7; Student's t-test: t=15.261, p<0.001. Fig. 2F). Because larger numbers of supplementary images were required for full connectome segmentation, the total dataset per muscle was naturally larger than that for YFP-H (16.2 ± 5.37GB (mean ± SD), range 8.3 – 22.01 vs. 6.81 ± 1.45GB, range 5.21 – 8.03; Student's t-test: t=3.095, p<0.01, Fig. 2G). The time taken to segment each motor unit in full connectomes was almost double that of YFP-H motor units (6.75 ± 1.76 hours (mean ± SD) vs. 3.00 ± 1.47 hours; Student's t-test: t=4.628, p<0.01, Fig. 2H) although there was no difference in the amount of data per motor unit (Fig. 2I).

Motor unit analysis

Identification of neuromuscular junctions (NMJs) occupied by each motor unit

Motor unit arbors were analysed by first inspecting the spread of occupied endplates through the MIP of each muscle. For this, reconstruction of segmented muscle images was merged with the TRITC-α-BTX image channel; each individual endplate was then labelled according to colocalising axon terminals. Very few endplates appeared to overlap on the MIPs. However, we separated these by comparing the MIP with with 2-channel 3D image stacks consisting of reconstructed motor units and endplates.

Characterisation of motor unit arbors

To measure the region infiltrated by each motor unit we used the polygon tool in Fiji to trace around the extremities of each motor unit arbor; and the area of this polygon was recorded. The polygon bounding the total complement of motor endplates was referred to as the 'endplate band'. Variability in endplate band area may have been accentuated by the squashing of muscles during preparation. To address this we normalised data where we predicted that muscle size or area would affect the analysis. We also recorded the coordinates of the approximate, subjectively estimated centre of each endplate, and calculated the centroid for the motor unit (defined as the mean *x* and *y* coordinates for the endplates occupied by that motor unit). We then determined the centroid for the region embracing all motor endplates in the muscle. Finally we measured the distance of each endplate from this centroid, the distance between motor unit and muscle centroids and the distance between motor

unit centroid and the point of nerve entry, defined as the first branching point of the nerve after entry into the muscle.

To calculate total arbor length (TAL), the length of each axon branch traced was measured using the Simple Neurite Tracer plugin in Fiji. For each motor unit the lengths of each axon branch were summated from the point of nerve entry into the muscle.

Motor unit branching symmetry

For each motor unit a dendrogram was generated to describe its branching pattern. To analyse branching symmetry, we used a modified version of Heard's imbalance index I (Heard, 1992) – described as $\Sigma_{\text{all interior nodes}}|T_R - T_L|/(n-1)(n-2)$, where T_R and T_L are the number of terminals distal to each branching node and n is the number of terminals within the motor unit. Because there were nodes that were tri-, 4- and 5-furcations it was necessary to adapt this metric in order to calculate the mean value of all pairwise differences at each branching node.

Endplate size analysis

To compare endplate sizes between and within muscles and motor units, we measured endplate length in its longest axis in the MIP. Endplates that appeared to be damaged or with ambiguous boundaries, for instance through overlap with their neighbours, were discounted. Length was measured using the line tool in Fiji.

Data processing and statistical analysis

All images and data were processed and analysed using a 2009 MacBook Pro (Intel Core 2 duo 2.53GHz processor, 8GB DDR3 RAM). Images were analysed using Fiji and Adobe Photoshop; spreadsheets and mathematical calculations were done in Microsoft Excel 2011 for Mac. Statistical comparisons were made in PASW 17, and graphs and charts were produced using GraphPad Prism 5. The choice of statistical test is described for each analysis within the text. For comparison between genotypes, YFP16 and CFP muscles were assumed to be equivalent and data was collated into a single YFP16/CFP group. Data are quoted as medians with ranges or, unless otherwise stated, mean ± standard deviation (SD).

RESULTS

Morphological features of the 4DL and its innervation

The number of motor neurons innervating YFP16 and CFP muscles ranged from 4-9 (median 6). The number of muscle fibres in 4DL muscles varied between 187 and 309 (median 242.5, IQR 198.25 – 279.25). Motor unit size, defined as the number of NMJs innervated by a motor unit, ranged from 3-111 (median 37.5, IQR 21.25 - 63.25). The area of muscle covered by motor endplates (endplate band area) was also highly variable (0.223 - 0.931mm^2, mean 0.480 ± 0.236). The distribution of motor unit size was positively skewed (Fig. 3). Overall, the motor unit size distribution observed in these complete connectomes (YFP16/CFP; Fig. 3C) closely resembles the distribution of motor unit sizes inferred from twitch tension experiments in rat lumbrical muscles (Betz *et al.*, 1979, 1980; Ridge & Rowlerson, 1996).

We also analysed fluorescent motor units in YFP-H muscles. We initially used these muscles to test and help develop our image segmentation protocol. For instance, they indicated the effect of innervation complexity on the amount of time required for image segmentation analysis (see Methods, and Fig 2). However, fluorescent motor unit size in YFP-H muscles was less skewed and ranged in size from 25-81 muscle fibres (median motor unit size, 49 muscle fibres). These units thus appeared to represent a specific subset of the population observed in 4DL muscles from YFP16 and CFP mice (A. Teriakidis, T. C. Hirst and R. R. Ribchester, in preparation). For that reason they were excluded from the analysis of motor unit size distribution in Fig. 3. However, since there was no *a priori* reason to exclude them on the basis of any other abnormality or type-specificity, the additional analysis contributed to the statistical confidence in our conclusions based on the data shown in Figs 4-6.

Many of the morphological properties we observed in the 4DL complement those previously reported in the interscutularis and others (Parson *et al.*, 1997; Lu *et al.*, 2009). For instance, these authors showed that branching of axons did not consistently coincide with fascicle branching, and branching of axons and fascicles was far from regular; the anatomy of each motor unit was very different to others even within a muscle. The same conclusions emerged from our analysis (Fig. 3A-B). Many axon branches followed tortuous routes and some ran in opposite directions to the majority of those in the same fascicle (Fig. 3A, asterisks), and fasciculation was complex (Fig. 3A, arrows), also in the same way as described previously (Lu *et al.*, 2009). We segmented one left-right pair of YFP16 muscles, and found different numbers of muscle fibres (190 vs. 240), motor units (5 vs. 4), and ranges of motor

unit sizes (left: 16 - 73; right: 45 - 65) – supporting the notion that motor units are not genetically determined like those in invertebrates (Macagno *et al.*, 1973; White *et al.*, 1986).

Similarly, branching of individual motor units did not initially appear to be systematically ordered. As previously described, the exact branching pattern of a motor axon varied between motor units of the same size. Dendrograms of axon branching were thus highly variable (Fig. 4A). Lu *et al* (2009) noted striking instances of pre-muscular axon branching, where nerves bifurcated into two branches containing motor axons that went on to innervate the muscle. However, we did not observe this in either of the two muscles that included a length nerve measuring around 1mm afferent to entering the muscle (data not shown; entry point into the muscle was defined as the first fascicle branch point). Branching of axons was most commonly binary, but with up to 5-furcations at some nodes. Of 1608 branching points identified, 1402 (87.2%) were bifurcations, 188 (11.7%) were trifurcations, 18 (1.12%) were 4-furcations and 4 (0.25%) were 5-furcations. While larger motor units contained more tri-, 4- and 5-furcations, the proportion of higher order branching points did not change with motor unit size.

To assess the branching symmetry of each motor unit, we used a modified version of Heard's Imbalance Index (see Methods; (Heard, 1992)), giving an output between 0 and 1 (0 denotes perfect symmetry and 1 perfect asymmetry of branching). Data from every motor unit was included, except for one of motor unit size 3, as this was too small to apply the metric. While index values ranged from 0.05 to 0.65 (n=41), there was a significant correlation between motor unit size and branching symmetry, with larger motor units branching more symmetrically as described in by Lu *et al* (linear regression: $F=21.2$, $df=40$; $R^2=0.346$, $p<0.001$, Fig. 4B).

Next, we measured the total arbor length (TAL) of each motor unit – defined as the summative length of all axon branches distal to its entry into the muscle. We also measured endplate band area (see Methods). We normalized TAL according to the muscle size (dividing by root-endplate band area) and the resulting regression with motor unit size was strong ($F=111$, $df=40$; $R^2=0.741$, $p<0.001$, Fig. 4C). Lu *et al* showed motor unit size and TAL to have a roughly inverse-square relationship. However, for the present data, curve fitting in SPSS favoured a linear relationship over other nonlinear options in this muscle.

Finally, Lu et al showed that axon caliber was correlated with motor unit size. We therefore attempted to measure axon caliber of motor axons immediately proximal to the first branch point. The point spread in the *z* axis of the images compromised resolution and accurate measurement in our images. However, we found no compelling evidence to reject or contrast the findings with those reported by Lu *et al* (data not shown).

Intrinsic features of motor neurons that define neuromuscular anatomy

A remarkable feature of the 4DL motor units that appears to set this muscle apart from the interscutularis muscle (Lu *et al.*, 2009) is that the arborisation and infiltration of motor units into the muscle showed evidence of hierarchical organisation. The largest motor units – i.e. those innervating the greatest number of NMJs in each muscle – commonly had multiple axon branches within the same nerve fascicle, occasionally occupying a whole fascicle and thus monopolising a portion of the muscle (5 motor units in 4 muscles: motor unit sizes 111, 86, 73, 61, and 55; these were all either the largest or second largest in the muscle. Fig. 5A, a & b). We also observed that small motor units, as well as having a smaller arbor area, often appeared limited to regions of the muscle close to the nerve entry point: 6 motor units from 4 muscles displayed this characteristic and in the small area that they did occupy, NMJs appeared to be densely clustered (Fig. 5B, a-c, green motor units (online)). One such motor unit formed two distinct, albeit separated clusters (Fig 5Bc, blue motor unit (online)).

To quantify the relationship between motor unit size and arborisation, we analysed the spread and location of each motor unit within the endplate band and the distribution of NMJs within the arbor. For instance, we wanted to establish whether small motor units (with the fewest NMJs) could have their connections dispersed throughout the muscle or focussed on a more clustered subset of muscle fibres. Initially we used the area of the polygon bounding the locations of NMJs of each motor unit as measure of dispersion (see Methods). We found that larger motor units occupied a significantly larger area within the muscle than smaller motor units. We then defined the proportion of a muscle occupied by a motor unit as the percentage area of the endplate band occupied by its arbor. Correlation between this statistic and motor unit size was significant (Spearman ρ=0.870, $p<0.001$, Fig. 5C). Interestingly, there was no correlation between the density of occupied endplates and motor unit size.

Next we examined motor units for systematic differences in the distribution of their axon branches. As an index, we calculated the centroids for each motor unit and for the muscle, in a MIP of that muscle. We then calculated the distance between each endplate and the motor unit centroid, normalised to the square root of the endplate band area of each muscle. We plotted these data against motor unit size. We found that these measures were significantly correlated, with larger motor units occupying larger areas (Fig. 5D; Spearman $\rho=0.557$, $p<0.001$). Correlation of motor unit size with the index of dispersion (defined as variance/mean) showed no relationship, however, suggesting that smaller motor units occupy NMJs at the same density but over a smaller area than their larger counterparts.

Finally, we asked whether the small motor units were selectively distributed. For instance, we wanted to establish whether small motor units were confined to the nerve entry point, as suggested by our qualitative description above. To evaluate this, we first measured the distance between motor unit centroid and the centroid of all NMJs in the muscle, normalised as above. There was again a significant correlation indicating that small motor units were more likely to be clustered near to the edge of the muscle (Spearman $\rho=-0.682$, $p<0.001$, Fig. 5E). Next we examined the relationship of motor units to the nerve entry point. We defined the point of nerve entry as the location where the muscle nerve first divided into branches. We then plotted the normalised distance between motor unit centroid and nerve entry point. This analysis indicated a significant correlation with motor unit size. Thus, smaller motor units preferentially occupy muscle fibres near the edge of the muscle but closest to the primary intramuscular nerve entry point (Spearman $\rho=-0.555$, $p<0.001$, Fig. 5F).

To summarise we obtained evidence for a size-dependent infiltration of motor units into the endplate band, with the largest motor units distributed evenly across the muscle and smaller motor units occupying concentrically smaller regions converging on the vicinity of the intramuscular nerve entry point. However, large motor units were not excluded from this zone. This may have implications for the process of developmental synapse elimination that establishes motor unit territories.

Does the distribution of 4DL motor units represent a dominance hierarchy?

Based on the above analysis, it is not possible to distinguish whether large motor units always have the competitive advantage, versus the alternative of random outcomes when small and large motor units compete for mononeuronal innervation of

individual muscle fibres during developmental synapse elimination(Brown & Ironton, 1976; Keller-Peck *et al.*, 2001; Walsh & Lichtman, 2003). For instance, if large motor units always dominated there would be no advantage to small motor units at the level of competition for innervation of individual motor endplates. On the other hand, if synapse elimination were a pseudorandom process, there would be no advantage to either these or any other motor unit whose initial distribution was independently determined. The outcome might be the same: selective distribution but no difference in the density of innervation in small or large motor units. Resolution of these possibilities is beyond the scope of the present study. However, we sought some insight by examining the sizes of motor endplates in relation to motor unit size. The reasoning is as follows. Previous studies of the generation of mononeuronal innervation patterns in muscle during postnatal development suggest that a combination of intrinsic (non-competitive) and competitive mechanisms direct the elimination of polyneuronal innervation (Brown & Ironton, 1976; Betz *et al.*, 1980; Fladby & Jansen, 1987). The outcome may be determined partly by differences in activity in the convergent axons and partly by differences in synaptic strength (Ribchester & Taxt, 1983; Costanzo *et al.*, 2000; Buffelli *et al.*, 2003; Kasthuri & Lichtman, 2003). Since there is also a well established relationship between between synaptic size and synaptic strength (Kuno *et al.*, 1971; Harris & Ribchester, 1979; Costanzo *et al.*, 1999), we compared endplate lengths within motor units as an indirect measure of synaptic strength and plotted these as a function of motor unit size.

We measured 2080 endplates in 39 motor units from 10 muscles (5 YFP-H, 3 YFP-16 and 2 CFP) .The median length of endplates was 32.5μm (IQR 26.7 – 37.4) and the distribution of lengths was positively skewed (Kolmogorov-Smirnov: Length $Z=2.92$, $p<0.001$, Fig. 6A). In order to permit parametric analysis of the data, we normalised the distribution of endplate lengths by plotting their log-transform.

Log endplate length showed significant heterogeneity between muscles, (ANOVA: $F=29.1$, $p<0.001$; Adjusted $R^2=0.108$, Fig. 6B). As mice were all either less than 15 weeks old (8 muscles) or over 40 weeks (2 muscles), we stratified the data into groups of less than 15 and over 40 weeks. As expected, the older group had significantly larger endplates than younger mice (1.51 ± 0.19 log units vs. 1.49 ± 0.11 log units; $p<0.01$ Student's t-test:). We also stratified by gender, and males were found to have larger endplates than females (1.55 ± 0.097 log units vs. 1.48 ± 0.10

log units; p<0.001, Student's t-test:). As there were three stratifications of the same dataset at this stage, we used Bonferroni correction to adjust cut-off significance to 0.017.

To investigate further the heterogeneity between motor units, we normalised log endplate length to account for between-muscle variance, permitting direct comparison of motor units from different muscles. We did this by multiplying each endplate length by the overall mean for the entire dataset divided by the mean value for the muscle. Between-motor unit heterogeneity accounted for a small but significant proportion (4.9%) of overall normalized endplate length variance (ANOVA: F=3.76, p<0.001; adjusted R^2=0.049, Fig. 6C). Therefore, while differences in endplate length between motor units were statistically significant, the majority of endplate length variability, over 95%, appeared to be within the parent motor units

Finally, we searched for a relationship between endplate length and motor unit size (Fig. 6D). The relationship between mean normalized log endplate length and motor unit size appeared curvilinear and there was no difficulty in fitting a polynomial equation to these data. That is, the smallest motor units (motor unit size <20) appeared to have notably smaller motor nerve terminals than large motor units. However, the scatter was large and we could define no model that would underlie a polynomial curve fit. We therefore simply calculated the correlation coefficient and linear regression. Endplate length correlated weakly but significantly with motor unit size (linear regression: F=8.54, *df*=39; R^2=0.187, p<0.01). This analysis suggests that motor unit size accounts for 18.7% of the variance in endplate length between motor units. On this basis we anticipate that during development larger motor units may have stronger synapses than small motor units and this property may be influential in determining the outcome of synapse elimination in accordance with a hierarchy of motor unit competitive strength. This hypothesis merits further investigation using more direct optical or electrophysiological methods to explore the possible relationship between motor unit size and intrinsic synaptic strength (Harris & Ribchester, 1979). (Tabares *et al.*, 2007; Ribchester, 2009; Ruiz *et al.*, 2011).

DISCUSSION

Understanding whether and how selectivity of motor innervation arises in normal development and how it is maintained through normal adult life may provide insight into how hierarchies of motor unit function arise and are maintained, for instance in

the orderly recruitment of motor units over a wide range of demands on motor function: the so-called 'size principle' (Henneman, 1985, 1991; Buffelli *et al.*, 2003; Kasthuri & Lichtman, 2003). Establishing such relationships could yield insight into organizational principles and mechanisms of synaptic and motor unit vulnerability following axonal injury or in disease. We analysed the 4DL muscle mainly because of its proven utility in physiological experiments, designed to establish the role of competition in the plasticity of motor units. The main advantage of 4DL in this regard arises from its unusual innervation by motor axons supplied by two anatomically distinct peripheral nerves: branches of the tibial and sural nerves which unite to form a homogeneous bundle of axons in the lateral plantar nerve (Betz *et al.*, 1979; Costanzo *et al.*, 2000; Ribchester *et al.*, 2004).

The main advances accomplished by the present study are first, an accelerated method for optical segmentation of the connectome, which we tested using the mouse 4th deep lumbrical muscle; a progressive resolution approach improved the efficiency of this segmentation as well as facilitating connectomic analysis, without dedicated hardware, software and personnel. This approach makes feasible a distributed, parallel approach to connectomic analysis where even small laboratories with limited resources could contribute effectively to connectomic analysis of even quite large muscles with complex innervation patterns.

Our second main finding was indirect evidence for motor unit hierarchies within the 4DL, which may have generated a concentric cylindrical segregation in the organization of motor units, with intermingling of large and small units but restriction of small unit arbors to the nerve entry point (Fig. 7). Previously, Gates & Betz (Gates & Betz, 1993) remarked upon the absence of connections with peripheral muscle fibres in some motor units in rat 4DL muscles, suggesting a restricted, non-random distribution of motor unit arbors. The present findings directly extend and add detail to this observation. Taken together, the data indicate an intriguing pattern of motor unit organization in 4DL that may turn out to be similar for other, apparently homogenously-innervated muscles.

Finally, we combined 4DL connectomic analysis with measurements of endplate size, an indirect measure of synaptic strength. The data, though only marginally significant statistically, warrants further investigation of relationships between motor unit order and synaptic strength, which may be of significance for neuromuscular development.

Efficiency of image segmentation

Significant steps have already been made in defining the connectomes of various tissues and relating their organization to their function: for example, in mouse retinal bipolar neurons (Helmstaedter *et al.*, 2011; Kleinfeld *et al.*, 2011) and in the plasticity of behavioural responses to olfactory stimuli in *C. elegans* (White *et al.*, 1986; Macosko *et al.*, 2009; Bendesky *et al.*, 2011). However in order to implement connectomics in deeper and more complex mammalian CNS tissue, improvements in speed and accuracy of neuropil segmentation will be required. The progressive resolution strategy we implemented here was a simple improvement that did not compromise resolution of connectivity. We provide a framework around which it is possible to quickly describe connectomes of single motor units or produce detailed analysis of complete small muscles. Other steps may be required to extend the method to larger muscles containing many fascicles. This method accommodates difficulties inherent to image segmentation in cylindrical muscles, and it reduces both the size of the dataset required and the time taken for analysis by permitting connectome segmentation from a single image and by streamlining data such that high resolution images are only used where necessary. Combination with public domain image analysis software renders connectomic segmentation more feasible for investigators with limited access to confocal microscopy. Further improvements might be achieved by intensity profiling and incorporating secondary images directly into the primary image stack, although such procedures would increase processing time. Applying connectomic analysis to immature or reinnervated adult muscles could yield further insights into the role of intrinsic neuronal properties and motor unit size in the outcome of synaptic competition (Costanzo *et al.*, 2000; Gillingwater *et al.*, 2002).

Hierarchical organization of 4DL motor units

Some characteristics of the 4DL connectome corroborated those noted previously in connectomic analysis of the interscutularis muscle, but we also identified a novel and surprising feature of motor unit organization in 4DL – namely a segregated concentric organisation of motor unit arbors.

Like interscutularis motor units, 4DL axon arbors that were not coordinated with fascicular branching, and axon branches were occasionally observed running in contraflow within a nerve fascicle (Fig. 3A, asterisks), consistent with the suboptimal wiring length reported by Lu *et al* (2009). We also identified discordance in several features of one bilateral pair of muscles, supporting their suggestion that there is no genetically determined neuromuscular organisation comparable to invertebrates. We

found that dendrograms of motor units were complex and variable and, as expected, total arbor length of a motor unit correlated strongly with motor unit size.

In addition, we obtained evidence for a hierarchical organization of motor axon arbors in 4DL. Specifically, the distribution of motor unit arbors suggests that the morphology of an arbor is dependent on motor unit size. Large motor units occupied NMJs throughout the muscle but smaller motor units were progressively and concentrically confined to smaller areas, with the smallest motor unit arbors restricted in distribution to the region close to the intramuscular nerve entry point. However, the large motor units are not excluded from these areas (see Fig. 3A-B). Analysis of axon arbors and a centroid-based clustering analysis corroborated these observations, implying that the spread of a motor unit arbor within the muscle is dependent on motor unit size. These findings are all summarized in Fig. 7, which encapsulates the main observations in the present paper.

Synaptic strength and motor unit size

Endplate length reflects synaptic strength, as larger endplates are associated with a larger quantal content and greater number of active zones (Harris & Ribchester, 1979). We therefore used endplate length as a first-approximation index of NMJ synaptic strength. Previous evidence (Buffelli *et al.*, 2003; Kasthuri & Lichtman, 2003) suggested that large motor units might be more successful during competitive elimination of neuromuscular synapses, suggesting that those motor units having the strongest synapses might also have the largest NMJs. The present data suggest that intrinsic properties of motor neurons may account for a small but significant proportion of endplate length heterogeneity in the adult 4DL. Motor unit size correlated weakly with mean endplate length, accounting for 18.7% of between-motor unit and 0.92% of overall endplate length heterogeneity. While we cannot make definitive conclusions from these preliminary data, we surmise from these measurements that these neuronal properties and synaptic strength at the adult NMJ may at least partially reflect that found during competitive synapse elimination in development. Further investigations, employing direct physiological measurements of synaptic strength will be required to validate our findings: for instance by immunostaining for active zones (Nishimune *et al.*, 2012), or using reporters of activity-dependent exocytosis, such as synaptopHluorin- or synaptophysin-pHluorin-based models (Granseth *et al.*, 2006; Tabares *et al.*, 2007).

AUTHOR CONTRIBUTIONS

Conception (RRR) and design (RRR/TCH) of experiments; collection (TCH), analysis (RRR/TCH) and interpretation (RRR/TCH) of data; drafting the article and revising it critically for important intellectual content (RRR/TCH).

ACKNOWLEDGEMENTS

We thank Dr Robert Hartley and Dr Adrianna Teriakidis for assistance with confocal microscopy and helpful discussions, Mr Derek Thomson for expert technical assistance, and Professor Thomas Gillingwater for helpful comments on the manuscript. Supported by the North British Hotels Trust, Medical Research Council and the Motor Neurone Disease Association.

REFERENCES

Barry JA & Ribchester RR. (1995). Persistent polyneuronal innervation in partially denervated rat muscle after reinnervation and recovery from prolonged nerve conduction block. *J Neurosci* 15, 6327-6339.

Bendesky A, Tsunozaki M, Rockman MV, Kruglyak L & Bargmann CI. (2011). Catecholamine receptor polymorphisms affect decision-making in C. elegans. *Nature* 472, 313-318.

Betz WJ, Caldwell JH & Ribchester RR. (1979). Post-natal development of motor units and muscle fibers in rat lumbrical muscles [proceedings]. *J Physiol* 289, 52P-53P.

Betz WJ, Caldwell JH & Ribchester RR. (1980). The effects of partial denervation at birth on the development of muscle fibres and motor units in rat lumbrical muscle. *J Physiol* 303, 265-279.

Betz WJ, Ribchester RR & Ridge RM. (1990). Competitive mechanisms underlying synapse elimination in the lumbrical muscle of the rat. *J Neurobiol* 21, 1-17.

Brown MC & Ironton R. (1976). The fate of motor axon sprouts in a partially denervated mouse muscle when regenerating nerve febres return [proceedings]. *J Physiol* 263, 181P-182P.

Buffelli M, Burgess RW, Feng G, Lobe CG, Lichtman JW & Sanes JR. (2003). Genetic evidence that relative synaptic efficacy biases the outcome of synaptic competition. *Nature* 424, 430-434.

Churchland PS & Sejnowski TJ. (1988). Perspectives on cognitive neuroscience. *Science* 242, 741-745.

Costanzo EM, Barry JA & Ribchester RR. (1999). Co-regulation of synaptic efficacy at stable polyneuronally innervated neuromuscular junctions in reinnervated rat muscle. *J Physiol* 521 Pt 2, 365-374.

Costanzo EM, Barry JA & Ribchester RR. (2000). Competition at silent synapses in reinnervated skeletal muscle. *Nat Neurosci* 3, 694-700.

Feng G, Mellor RH, Bernstein M, Keller-Peck C, Nguyen QT, Wallace M, Nerbonne JM, Lichtman JW & Sanes JR. (2000). Imaging neuronal subsets in transgenic mice expressing multiple spectral variants of GFP. *Neuron* 28, 41-51.

Fladby T & Jansen JK. (1987). Postnatal loss of synaptic terminals in the partially denervated mouse soleus muscle. *Acta Physiol Scand* 129, 239-246.

Gates HJ & Betz WJ. (1993). Spatial distribution of muscle fibers in a lumbrical muscle of the rat. *Anat Rec* 236, 381-389.

Gates HJ & Ridge RM. (1992). The importance of competition between motoneurones in developing rat muscle; effects of partial denervation at birth. *J Physiol* 445, 457-472.

Gates HJ, Ridge RM & Rowlerson A. (1991). Motor units of the fourth deep lumbrical muscle of the adult rat: isometric contractions and fibre type compositions. *J Physiol* 443, 193-215.

Gillingwater TH, Ingham CA, Coleman MP & Ribchester RR. (2003). Ultrastructural correlates of synapse withdrawal at axotomized neuromuscular junctions in mutant and transgenic mice expressing the Wld gene. *J Anat* 203, 265-276.

Gillingwater TH & Ribchester RR. (2003). The relationship of neuromuscular synapse elimination to synaptic degeneration and pathology: insights from WldS and other mutant mice. *J Neurocytol* 32, 863-881.

Gillingwater TH, Thomson D, Mack TG, Soffin EM, Mattison RJ, Coleman MP & Ribchester RR. (2002). Age-dependent synapse withdrawal at axotomised neuromuscular junctions in Wld(s) mutant and Ube4b/Nmnat transgenic mice. *J Physiol* 543, 739-755.

Granseth B, Odermatt B, Royle SJ & Lagnado L. (2006). Clathrin-mediated endocytosis is the dominant mechanism of vesicle retrieval at hippocampal synapses. *Neuron* 51, 773-786.

Harris JB & Ribchester RR. (1979). The relationship between end-plate size and transmitter release in normal and dystrophic muscles of the mouse. *J Physiol* 296, 245-265.

Heard SB. (1992). Patterns in tree balance among cladistic, phenetic, and randomly generated phylogenetic trees. *Evolution* 46, 1818-1826.

Helmstaedter M, Briggman KL & Denk W. (2011). High-accuracy neurite reconstruction for high-throughput neuroanatomy. *Nat Neurosci* 14, 1081-1088.

Henneman E. (1985). The size-principle: a deterministic output emerges from a set of probabilistic connections. *J Exp Biol* 115, 105-112.

Henneman E. (1991). The size principle and its relation to transmission failure in Ia projections to spinal motoneurons. ***Ann N Y Acad Sci*** **627, 165-168.**

Hennig R & Lomo T. (1985). Firing patterns of motor units in normal rats. ***Nature*** **314, 164-166.**

Hennig R & Lomo T. (1987). Gradation of force output in normal fast and slow muscles of the rat. ***Acta Physiol Scand*** **130, 133-142.**

Jones SP, Ridge RM & Rowlerson A. (1987). The non-selective innervation of muscle fibres and mixed composition of motor units in a muscle of neonatal rat. ***J Physiol*** **386, 377-394.**

Kasthuri N & Lichtman JW. (2003). The role of neuronal identity in synaptic competition. ***Nature*** **424, 426-430.**

Keller-Peck CR, Feng G, Sanes JR, Yan Q, Lichtman JW & Snider WD. (2001). Glial cell line-derived neurotrophic factor administration in postnatal life results in motor unit enlargement and continuous synaptic remodeling at the neuromuscular junction. ***J Neurosci*** **21, 6136-6146.**

Kleinfeld D, Bharioke A, Blinder P, Bock DD, Briggman KL, Chklovskii DB, Denk W, Helmstaedter M, Kaufhold JP, Lee WC, Meyer HS, Micheva KD, Oberlaender M, Prohaska S, Reid RC, Smith SJ, Takemura S, Tsai PS & Sakmann B. (2011). Large-scale automated histology in the pursuit of connectomes. ***J Neurosci*** **31, 16125-16138.**

Kuno M, Turkanis SA & Weakly JN. (1971). Correlation between nerve terminal size and transmitter release at the neuromuscular junction of the frog. ***J Physiol*** **213, 545-556.**

Lichtman JW & Denk W. (2011). The big and the small: challenges of imaging the brain's circuits. ***Science*** **334, 618-623.**

Lu J, Tapia JC, White OL & Lichtman JW. (2009). The interscutularis muscle connectome. ***PLoS Biol*** **7, e32.**

Macagno ER, Lopresti V & Levinthal C. (1973). Structure and development of neuronal connections in isogenic organisms: variations and similarities in the optic system of Daphnia magna. ***Proc Natl Acad Sci U S A*** **70, 57-61.**

Macosko EZ, Pokala N, Feinberg EH, Chalasani SH, Butcher RA, Clardy J & Bargmann CI. (2009). A hub-and-spoke circuit drives pheromone attraction and social behaviour in C. elegans. ***Nature*** **458, 1171-1175.**

Meinertzhagen IA & Lee CH. (2012). The genetic analysis of functional connectomics in Drosophila. *Adv Genet* 80, 99-151.

Murray LM, Comley LH, Thomson D, Parkinson N, Talbot K & Gillingwater TH. (2008). Selective vulnerability of motor neurons and dissociation of pre- and post-synaptic pathology at the neuromuscular junction in mouse models of spinal muscular atrophy. *Hum Mol Genet* 17, 949-962.

Nakanishi T & Norris FH, Jr. (1970). Motor fibers in rat sural nerve. *Exp Neurol* 26, 433-435.

Nishimune H, Numata T, Chen J, Aoki Y, Wang Y, Starr MP, Mori Y & Stanford JA. (2012). Active zone protein Bassoon co-localizes with presynaptic calcium channel, modifies channel function, and recovers from aging related loss by exercise. *PLoS One* 7, e38029.

Parson SH, Mackintosh CL & Ribchester RR. (1997). Elimination of motor nerve terminals in neonatal mice expressing a gene for slow wallerian degeneration (C57Bl/Wlds). *Eur J Neurosci* 9, 1586-1592.

Peyronnard JM & Charron L. (1982). Motor and sensory neurons of the rat sural nerve: a horseradish peroxidase study. *Muscle Nerve* 5, 654-660.

Pun S, Sigrist M, Santos AF, Ruegg MA, Sanes JR, Jessell TM, Arber S & Caroni P. (2002). An intrinsic distinction in neuromuscular junction assembly and maintenance in different skeletal muscles. *Neuron* 34, 357-370.

Ribchester RR. (1988). Activity-dependent and -independent synaptic interactions during reinnervation of partially denervated rat muscle. *J Physiol* 401, 53-75.

Ribchester RR. (2009). Mammalian neuromuscular junctions: modern tools to monitor synaptic form and function. *Curr Opin Pharmacol* 9, 297-305.

Ribchester RR & Taxt T. (1983). Motor unit size and synaptic competition in rat lumbrical muscles reinnervated by active and inactive motor axons. *J Physiol* 344, 89-111.

Ribchester RR, Thomson D, Wood NI, Hinks T, Gillingwater TH, Wishart TM, Court FA & Morton AJ. (2004). Progressive abnormalities in skeletal muscle and neuromuscular junctions of transgenic mice expressing the Huntington's disease mutation. *Eur J Neurosci* 20, 3092-3114.

Ridge RM & Rowlerson A. (1996). Motor units of juvenile rat lumbrical muscles and fibre type compositions of the glycogen-depleted component. ***J Physiol*** **497 (Pt 1), 199-210.**

Ruiz R, Cano R, Casanas JJ, Gaffield MA, Betz WJ & Tabares L. (2011). Active zones and the readily releasable pool of synaptic vesicles at the neuromuscular junction of the mouse. ***J Neurosci*** **31, 2000-2008.**

Srinivasan R, Li Q, Zhou X, Lu J, Lichtman J & Wong ST. (2010). Reconstruction of the neuromuscular junction connectome. ***Bioinformatics*** **26, i64-70.**

Tabares L, Ruiz R, Linares-Clemente P, Gaffield MA, Alvarez de Toledo G, Fernandez-Chacon R & Betz WJ. (2007). Monitoring synaptic function at the neuromuscular junction of a mouse expressing synaptopHluorin. ***J Neurosci*** **27, 5422-5430.**

Taxt T. (1983). Cross-innervation of fast and slow-twitch muscles by motor axons of the sural nerve in the mouse. ***Acta Physiol Scand*** **117, 331-341.**

Teriakidis A, Willshaw DJ & Ribchester RR. (2012). Prevalence and elimination of sibling neurite convergence in motor units supplying neonatal and adult mouse skeletal muscle. ***J Comp Neurol*** **520, 3203-3216.**

Walsh MK & Lichtman JW. (2003). In vivo time-lapse imaging of synaptic takeover associated with naturally occurring synapse elimination. ***Neuron*** **37, 67-73.**

White JG, Southgate E, Thomson JN & Brenner S. (1986). The structure of the nervous system of the nematode Caenorhabditis elegans. ***Philos Trans R Soc Lond B Biol Sci*** **314, 1-340.**

FIGURE LEGENDS

Figure 1 – Flowchart outlining the resolution of areas of ambiguity. A: YFP-H muscles. Areas of ambiguity, identified by manual inspection of the original image stack, were deconvolved to increase contrast and, failing this, reimaged with a 63x 1.4 NA objective. Once all areas were resolved the muscle was segmented using the original image stack. B: YFP16 and CFP muscles. Areas of ambiguity, identified by inspection of the original image stack, were defined as simple or complex according to the number of incoming axon branches. Simple areas were resolved using deconvolution or secondarily by reimaging as above; complex areas were reimaged without prior deconvolution. In some cases where ambiguity still remained these high power images were deconvolved. Once all areas had been resolved the connectome was segmented from the original image stack. If a muscle of either genotype contained areas of ambiguity that could not be resolved using this method, the sample was discarded.

Figure 2 – Axon tracing in low power images, identification of areas of ambiguity and their resolution. A: Full connectomes were segmented from a single merged image of the entire muscle (40x lens, voxel size 0.2x0.2x0.8µm). Much of the muscle, including major nerve fascicles, was segmented without further processing (white; B, E). Some areas required higher contrast or resolution, obtained by either deconvolution (upper box (yellow online); C, right) or by reimaging with a 63x, 1.4 NA objective (lower box (red online); D, right. See Methods). B: Orthogonal view of a cross-section of the intramuscular nerve showing sufficient contrast for a user to distinguish between axons, particularly when viewed as a series. C: Deconvolution (DC) of a simple area of ambiguity: left, original image; right, deconvolved image. Marked improvements in contrast can be seen both in MIP (top left vs. top right) and orthogonal cross section (bottom panels). D: Similar improvements on reimaging of a complex area of ambiguity (top left) at higher resolution using a 63x objective (top right), also showing improved resolution of ambiguity in orthogonal sections (bottom panels). E: Cross section of the primary nerve fascicle showing nine distinguishable motor axons entering the muscle. F: YFP-H muscles were significantly quicker to segment as a whole ($p<0.001$). G: Full connectomes required significantly more data than YFP-H muscles ($p<0.01$). H: The analysis time per motor unit was greater for full connectomes than for YFP-H muscles ($p<0.05$). I: The dataset required per motor unit was no different between YFP16/CFP and YFP-H muscles. Images presented in C and D simply represent those that are the result of deconvolution (C) or reimaging (D).

Figure 3 – Connectome of CFP-expressing muscle. A: Connectome constructed from renderings of individual motor units overlaid on a MIP of the muscle (top). The MIP is a combination of CFP and TRITC-α-BTX images, followed by median and gamma filtering to reduce noise and show the boundaries of the muscle by autofluorescence respectively. The complex pattern of fascicle branching and anastomosis in the muscle is easy to see (arrows) and asterisks show examples of axons in contraflow (see text). B: Each motor unit from the montage is rendered individually, revealing stochastic patterns of arborisation. Numbers represent the motor unit size of each motor unit. Red (online) colouration denotes the largest motor unit, with green (online) the smallest. C: Histogram of motor unit sizes for all motor units segmented from YFP16 and CFP muscles. The data are positively skewed. We excluded YFP-H units from this particular analysis for reasons given in the text.

Figure 4 – Branching properties of motor unit arbors. A: Two dendrograms of motor units close to the median in size (MU sizes 38 and 39): here the complex and variable branching patterns can be seen, as well as some examples of trifurcations (two examples indicated by arrows). B: Correlation of motor unit size with imbalance index I. Larger motor units branched more symmetrically ($p<0.001$). C: Total arbour length (TAL), normalised to the size of the muscle (root endplate band area, see Results), correlated linearly with motor unit size ($p<0.001$).

Figure 5 – Non-random motor unit arborisation. A: Monopolization of nerve fascicles by larger motor units. In 4 of 5 full connectomes, the largest motor units occupied an entire nerve fascicle, thereby monopolizing a cluster of motor endplates. These motor units were all either the second largest (Aa; orange (online), arrowed) or largest (Ab; red (online), arrowed) in that muscle. B: 4 of 5 muscles contained at least one motor unit that was confined to the portion of the muscle closest to the nerve entry point (examples from three different muscles are shown in panels a to c). Within these small regions, occupied NMJs appeared to be clustered quite densely. In Biii, one motor unit (blue, online) penetrated the muscle deeply but the NMJs that it occupied formed two clusters. C: Motor unit size correlated significantly with the percentage of endplate band occupied (Spearman $p<0.001$). D: Localisation of motor unit arbours: scatter plot showing motor unit size versus mean distance between NMJs and the centroid of NMJs for that motor unit, suggesting a positive relationship between motor unit arbor area and motor unit size (Spearman $p<0.001$). E: Locations of motor unit arbors within the muscle. Plot showing motor unit size versus the distance between MU centroid and overall muscle centroid showing smaller motor units to be located peripherally within the muscle (Spearman $p<0.001$). F: Distance between motor unit centroid and point of nerve entry, correlated with motor unit size demonstrating that small motor unit arbors are located closer to the intramuscular nerve entry point (Spearman $p<0.001$). Bars in D represent SEM; solid lines are best fit and dashed 95%CI of the regression. Lines of best fit were generated using the models $y=ax^b+c$.

Figure 6 – Endplate morphology. A: Collation of the lengths of 2080 endplates from 9 muscles showed a median length of 32.5µm (IQR 26.7 – 37.4) and the distribution was significantly skewed (Kolmogorov-Smirnov $p<0.001$). Therefore for further analysis, data was log transformed. B: Endplate lengths were significantly different between muscles (ANOVA $p<0.001$). For further analysis log endplate lengths were normalized to account for between-muscle variability. C: Normalised log endplate length varied significantly between motor units: between-motor unit variance accounted for 4.9% of between-motor unit endplate length variability (ANOVA: $p<0.001$, adjusted $R^2=0.049$). D: Mean normalized root endplate length varied with motor unit size (linear regression: $p<0.01$, $R^2=0.189$), suggesting a small but significant correlation between motor unit size and endplate size. Points in D represent mean ± SEM normalized log endplate length for each motor unit; dashed lines represent 95%CI of the regression.

Figure 7 – Diagrammatic representation of segregated concentric arborisation of motor units in mouse 4DL muscle. Left: 4th deep lumbrical with motor nerve supply (LPN: lateral plantar nerve, SN: sural nerve, TN: tibial nerve). Right: representation of motor unit arborisation in a schematic cross section through the muscle. The entering nerve is coloured black and motor units arbors are assembled concentrically around it, with arbor area in approximate proportion to motor unit size.

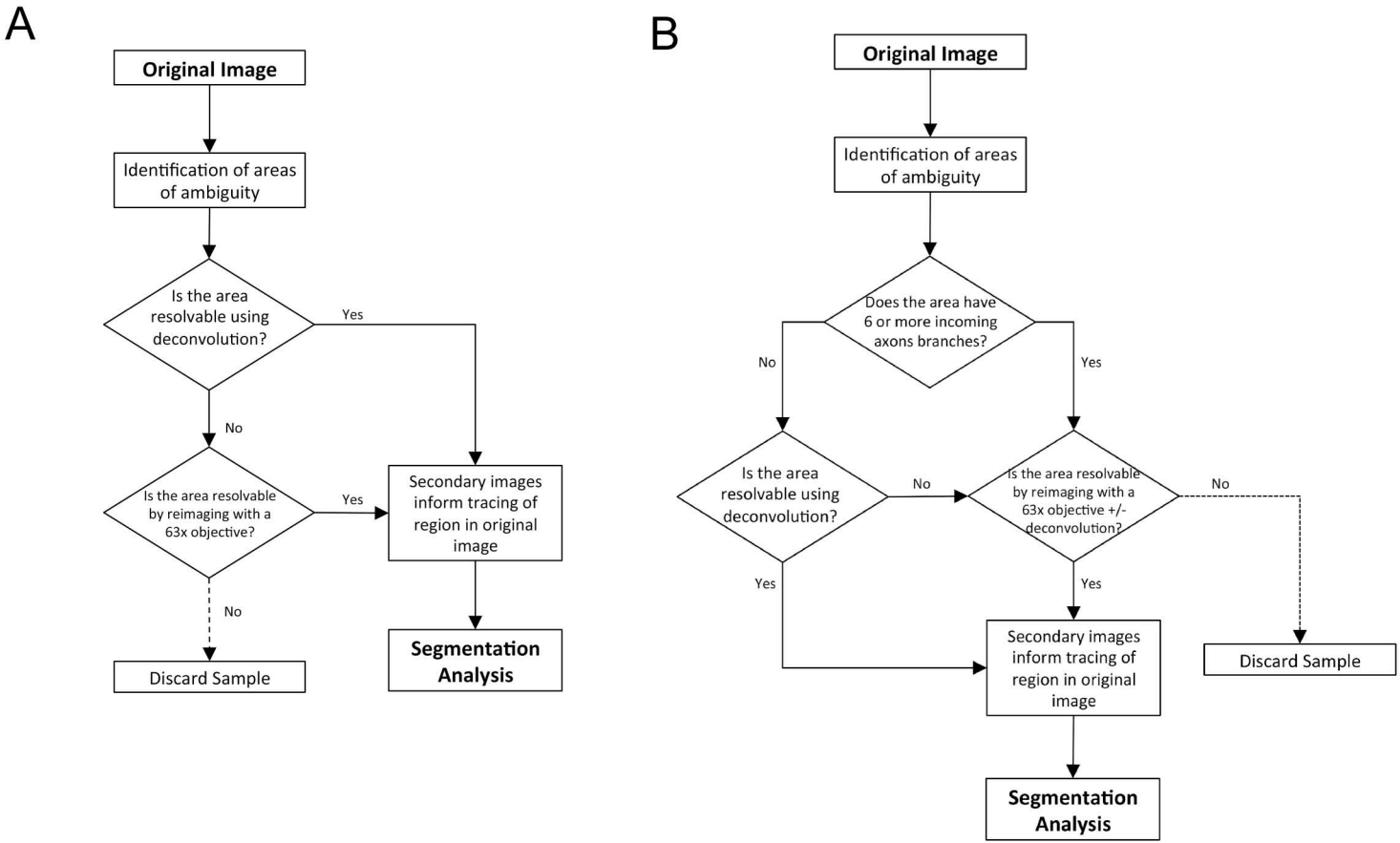
A
Original Image
Identification of areas of ambiguity
Is the area resolvable using deconvolution?
Yes
No
Is the area resolvable by reimaging with a 63x objective?
Yes
No
Secondary images inform tracing of region in original image
Discard Sample
Segmentation Analysis
B
Original Image
Identification of areas of ambiguity
Does the area have 6 or more incoming axons branches?
No
Yes
Is the area resolvable using deconvolution?
No
Is the area resolvable by reimaging with a 63x objective +/- deconvolution?
No
Yes
Yes
Secondary images inform tracing of region in original image
Discard Sample
Segmentation Analysis

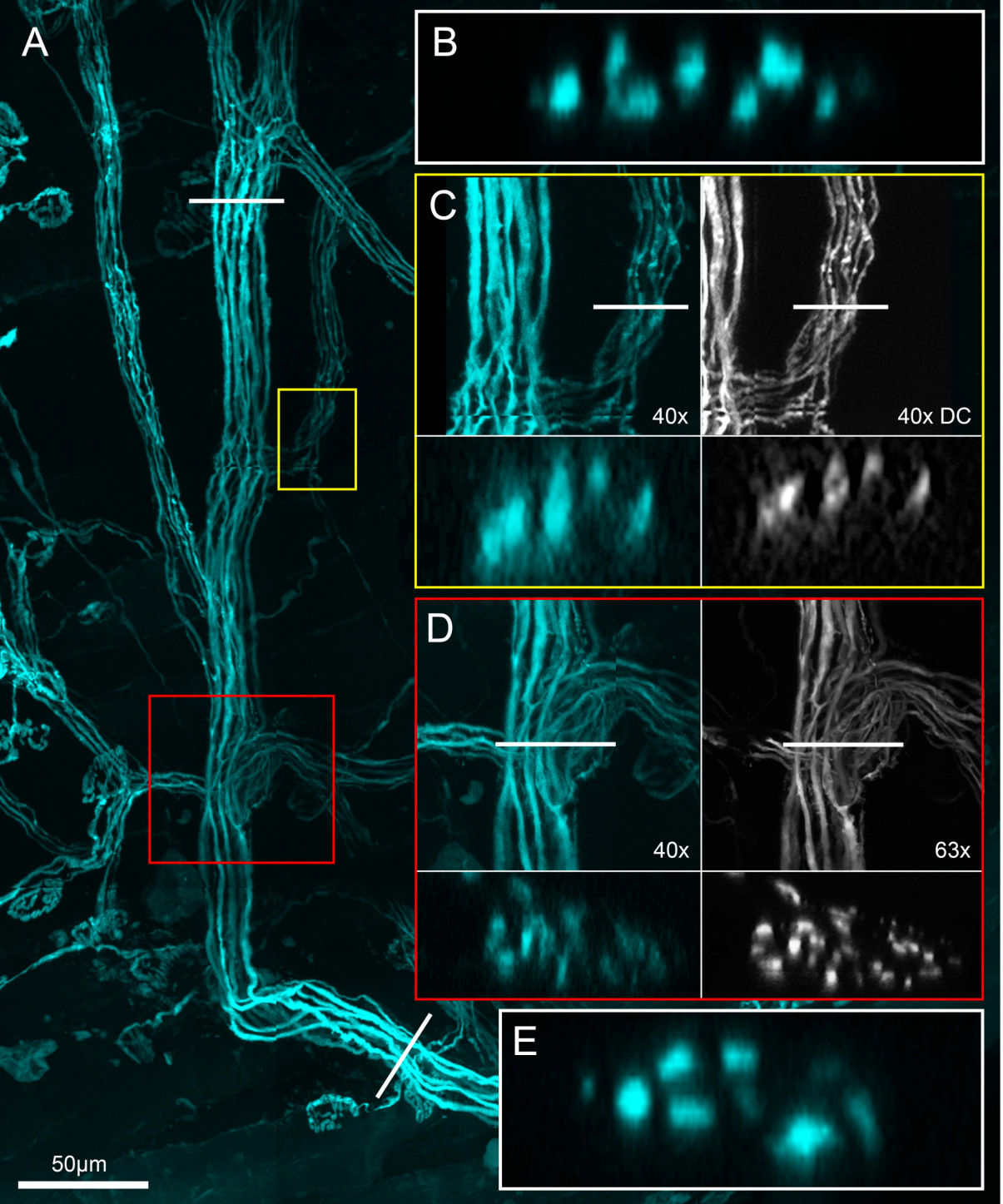
A
B
C
40x
40x DC
D
40x
63x
E
50µm

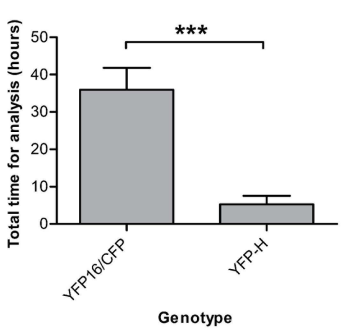
F
***
Total time for analysis (hours)
50
40
30
20
10
0
YFP16/CFP
YFP-H
Genotype

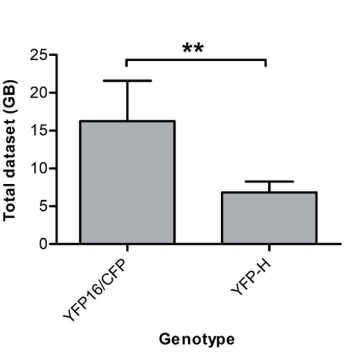
G
**
Total dataset (GB)
25
20
15
10
5
0
YFP16/CFP
YFP-H
Genotype

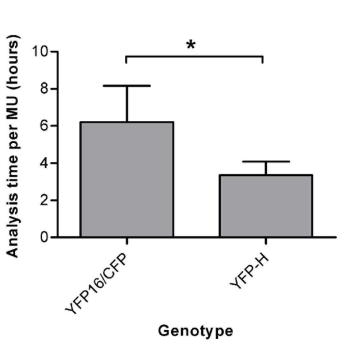
H
*
Analysis time per MU (hours)
10
8
6
4
2
0
YFP16/CFP
YFP-H
Genotype

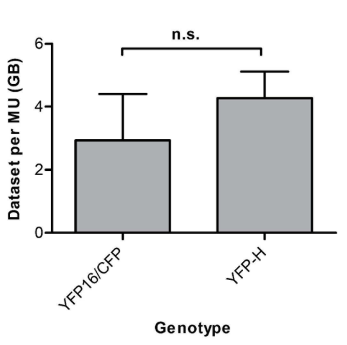
I
n.s.
Dataset per MU (GB)
6
4
2
0
YFP16/CFP
YFP-H
Genotype

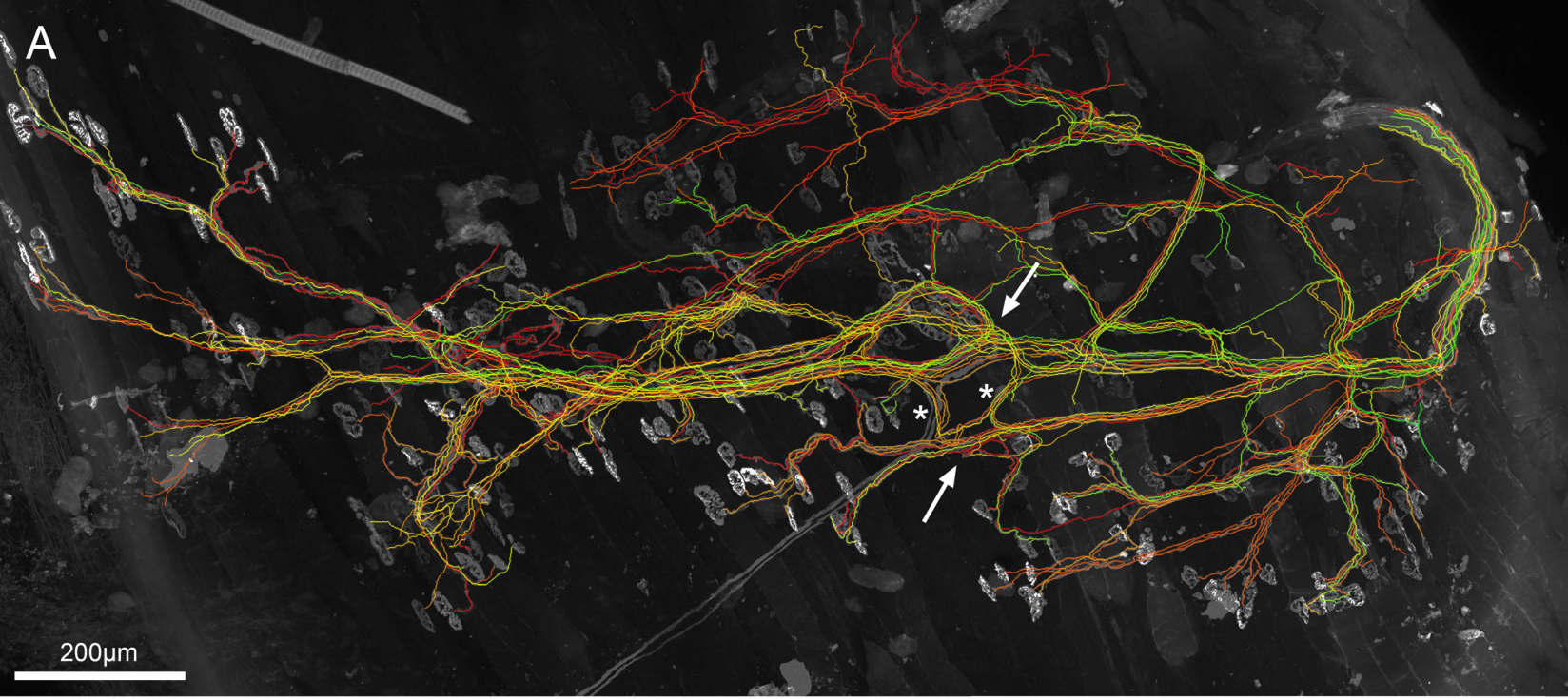
A
200µm

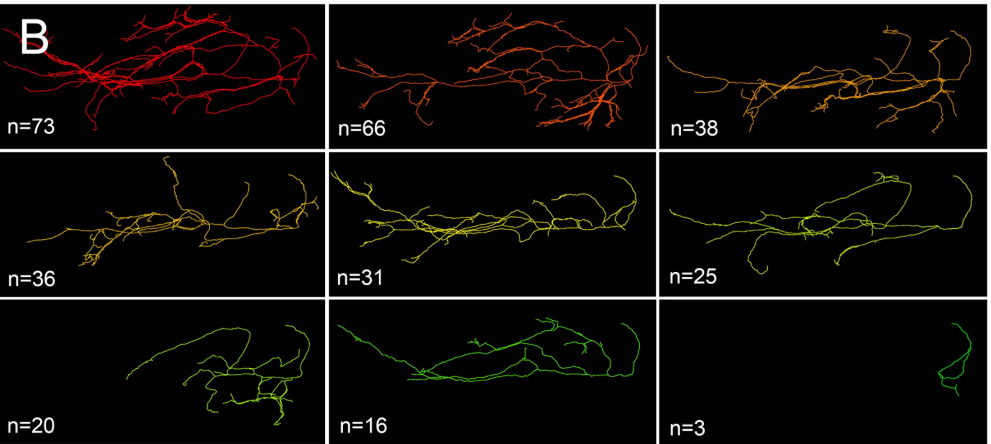
B
n=73
n=66
n=38
n=36
n=31
n=25
n=20
n=16
n=3

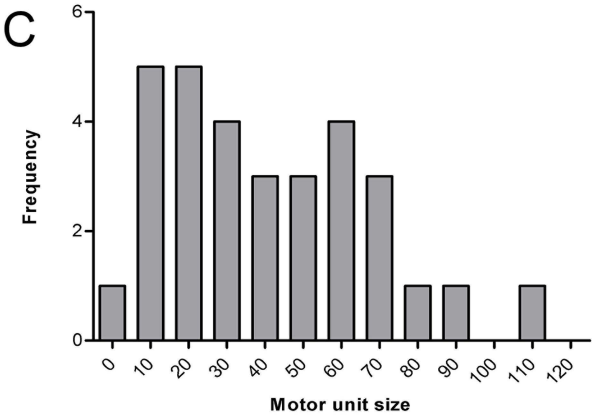
C
Frequency
0
2
4
6
0
10
20
30
40
50
60
70
80
90
100
110
120
Motor unit size

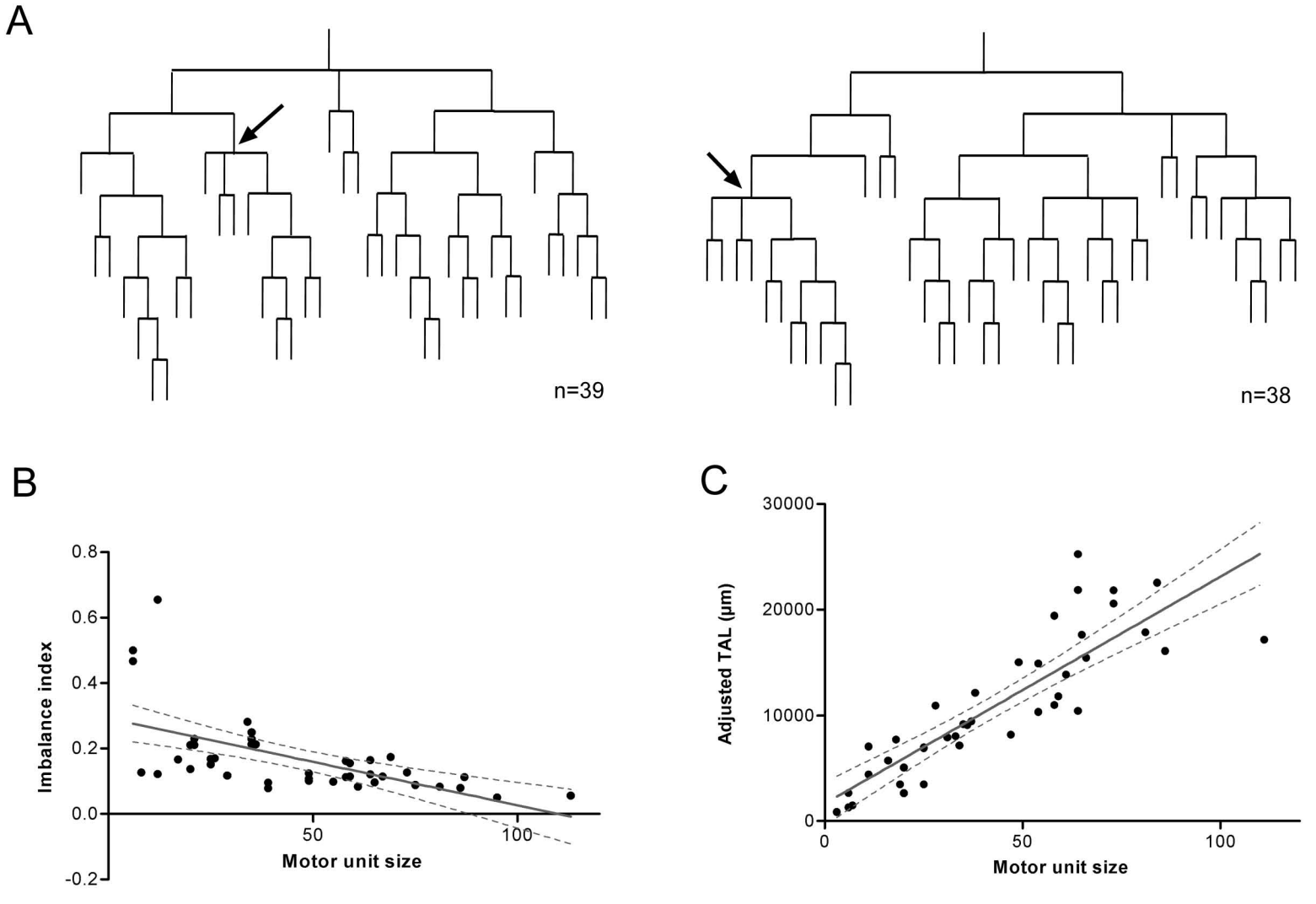
A
n=39
n=38
B
Imbalance index
0.8
0.6
0.4
0.2
0.0
-0.2
50
100
Motor unit size
C
Adjusted TAL (µm)
30000
20000
10000
0
0
50
100
Motor unit size

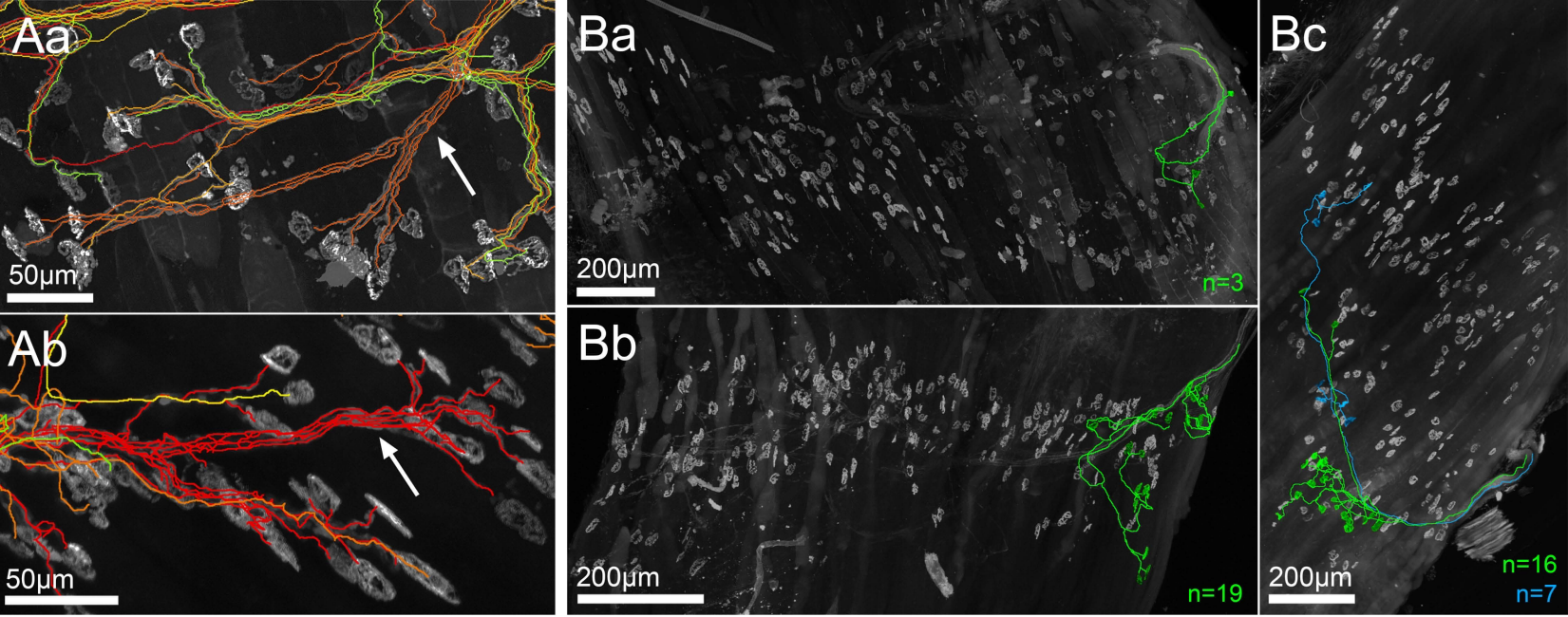
Aa
50µm
Ab
50µm
Ba
200µm
n=3
Bb
200µm
n=19
Bc
200µm
n=16
n=7

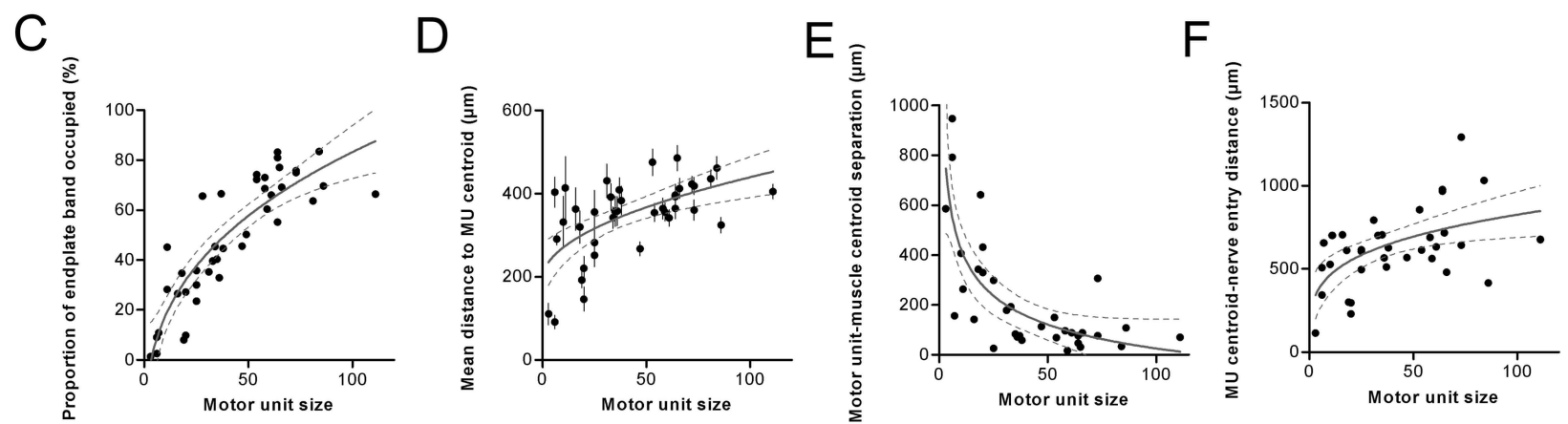
C
Proportion of endplate band occupied (%)
Motor unit size
D
Mean distance to MU centroid (µm)
Motor unit size
E
Motor unit-muscle centroid separation (µm)
Motor unit size
F
MU centroid-nerve entry distance (µm)
Motor unit size

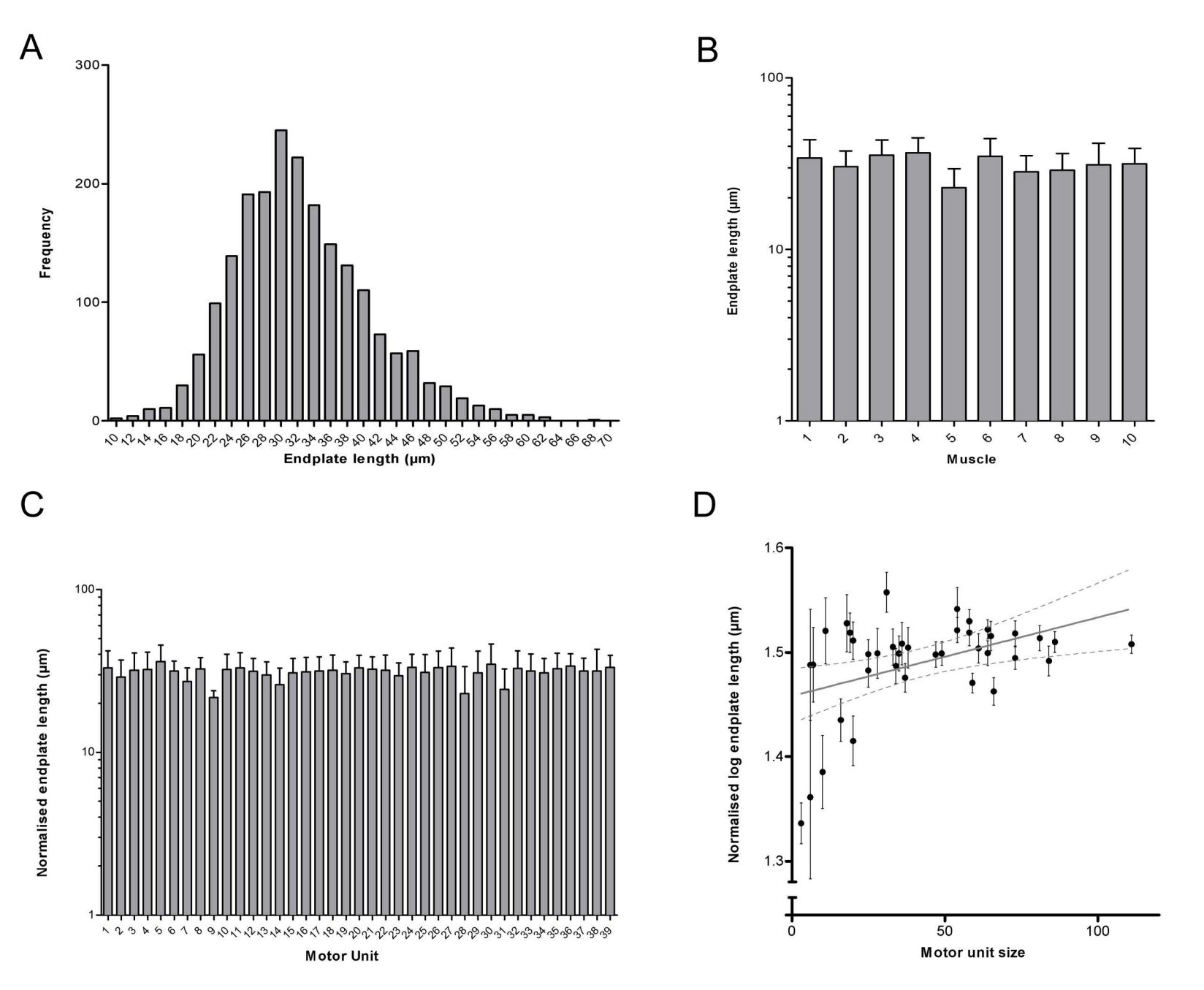
A
Frequency
Endplate length (µm)
B
Endplate length (µm)
Muscle
C
Normalised endplate length (µm)
Motor Unit
D
Normalised log endplate length (µm)
Motor unit size

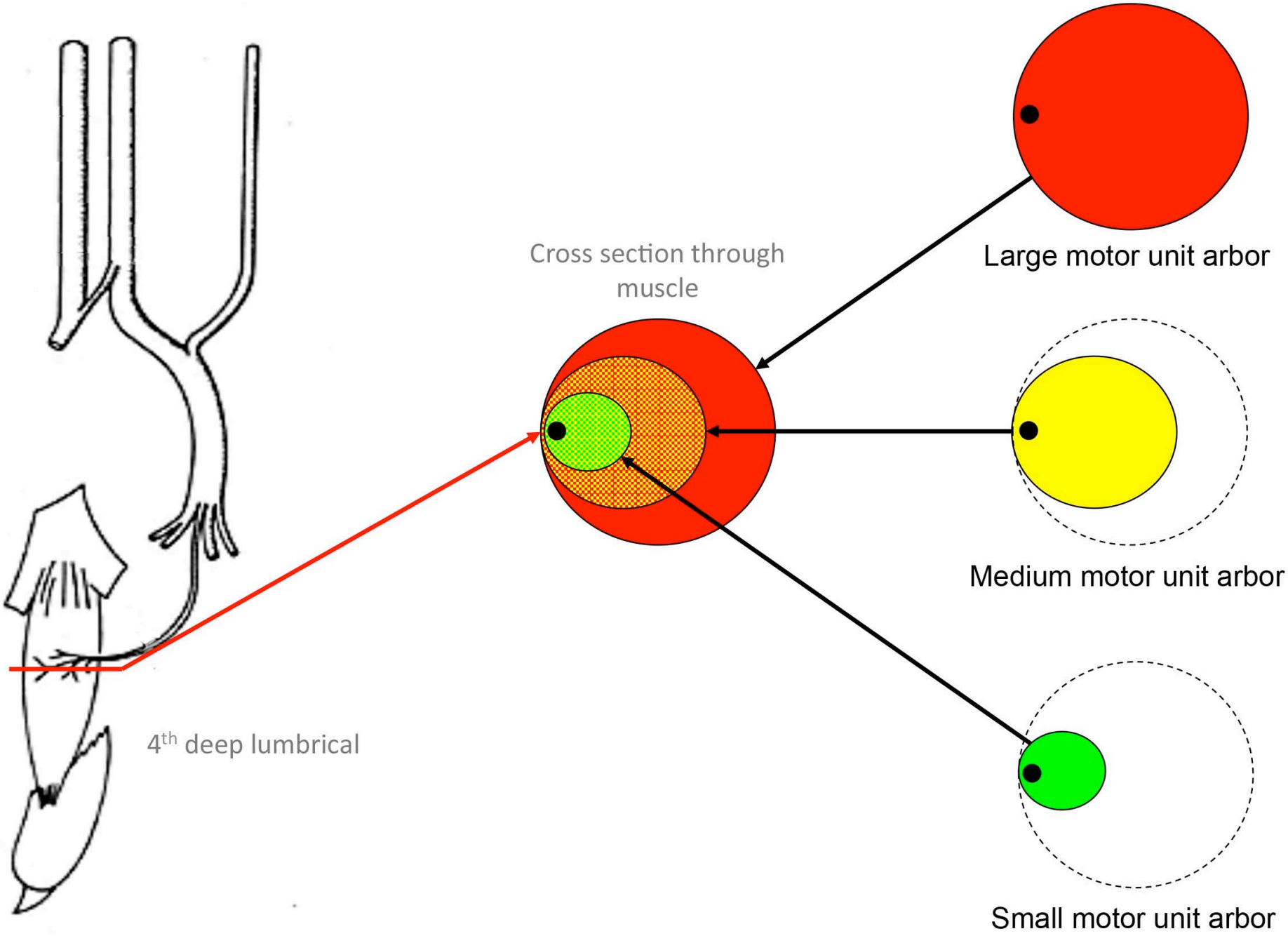
Cross section through muscle
Large motor unit arbor
Medium motor unit arbor
Small motor unit arbor
4th deep lumbrical